
Stabilizing GAN Training with Multiple Random Projections

Behnam Neyshabur Srinadh Bhojanapalli Ayan Chakrabarti
 Toyota Technological Institute at Chicago
 6045 S. Kenwood Ave., Chicago, IL 60637
 {bneyshabur, srinadh, ayanc}@ttic.edu

Abstract

Training generative adversarial networks is unstable in high-dimensions when the true data distribution lies on a lower-dimensional manifold. The discriminator is then easily able to separate nearly all generated samples leaving the generator without meaningful gradients. We propose training a single generator simultaneously against an array of discriminators, each of which looks at a different random low-dimensional projection of the data. We show that individual discriminators then provide stable gradients to the generator, and that the generator learns to produce samples consistent with the full data distribution to satisfy all discriminators. We demonstrate the practical utility of this approach experimentally, and show that it is able to produce image samples with higher quality than traditional training with a single discriminator.

1 Introduction

Generative adversarial networks (GANs), introduced by [1], endow neural networks with the ability to express distributional outputs. The framework includes a generator network that is tasked with producing samples from some target distribution, given as input a (typically low dimensional) noise vector drawn from a simple known distribution, and possibly conditional side information. The generator learns to generate such samples, not by directly looking at the data, but through adversarial training with a discriminator network that seeks to differentiate real data from those generated by the generator. To satisfy the objective of “fooling” the discriminator, the generator eventually learns to produce samples with statistics that match those of real data.

In regression tasks where the true output is ambiguous, GANs provide a means to simply produce an output that is plausible (with a single sample), or to explicitly model that ambiguity (through multiple samples). In the latter case, they provide an attractive alternative to fitting distributions to parametric forms during training, and employing expensive sampling techniques at the test time. In particular, conditional variants of GANs have shown to be useful for tasks such as in-painting [2], and super-resolution [3]. Recently, [4] demonstrated that GANs can be used to produce plausible mappings between a variety of domains—including sketches and photographs, maps and aerial views, segmentation masks and images, *etc.* GANs have also found uses as a means of un-supervised learning, with latent noise vectors and hidden-layer activations of the discriminators proving to be useful features for various tasks [2, 5, 6].

Despite their success, training GANs to generate high-dimensional data (such as large images) is challenging. Adversarial training between the generator and discriminator involves optimizing a min-max objective. This is typically carried out by gradient-based updates to both networks, and the generator is prone to divergence and mode-collapse as the discriminator begins to successfully distinguish real data from generated samples with high confidence. Researchers have tried to address this instability and train better generators through several techniques. [7] proposed explicitly factorizing generating an image into a sequence of conditional generations of levels of a Laplacian

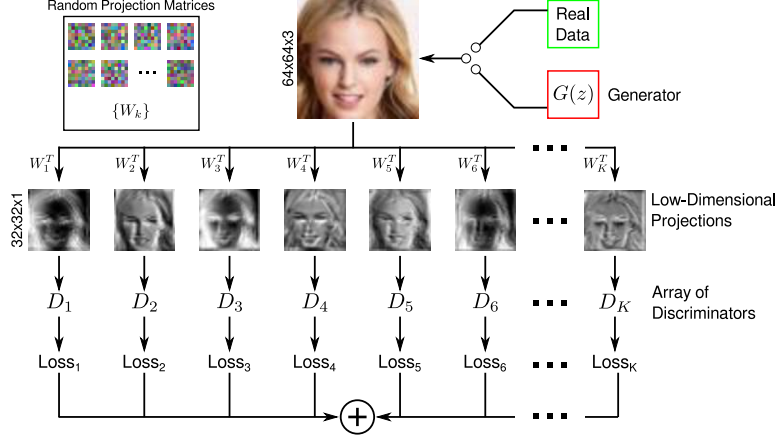


Figure 1: Overview of our approach. We train a single generator against an array of discriminators, each of which receives lower-dimensional projections—chosen randomly prior to training—as input. Individually, these discriminators are unable to perfectly separate real and generated samples, and thus provide stable gradients to the generator throughout training. In turn, by trying to fool all the discriminators simultaneously, the generator learns to match the true full data distribution.

pyramid, while [6] demonstrated that specific architecture choices and parameter settings led to higher-quality samples. Other techniques include providing additional supervision [8], adding noise to the discriminator input [9], as well as modifying or adding regularization to the training objective functions [10–12].

In this work, we seek to provide a framework that addresses a key source of instability [9] when training GANs—when the true distribution of high-dimensional data is concentrated in a small fraction of the ambient space. During training in such settings, the generator’s samples have very little overlap with the true distribution. This allows the discriminator to easily separate real and generated data perfectly. The generator then no longer receives any significant gradients from the discriminator to update its model, irrespective of its distance from the real data distribution.

To address this, we propose training the generator against an array of discriminators, each of which looks at a different, randomly-chosen, low-dimensional projection of the data. Each discriminator is unable to perfectly separate real and generated samples since it only gets a partial view of these samples. At the same time, to satisfy its objective of fooling *all* discriminators, the generator learns to match the true full data distribution. We formalize this intuition by providing results that show the marginals of the true data distribution along the lower-dimensional projections are less concentrated, effectively alleviating the problem of vanishing gradients for each discriminator. Furthermore, we show that with discriminators trained on different random projections, the generator will learn a distribution that well approximates the true data distribution. Finally, we demonstrate the efficacy of our approach by using it to train generators on standard image datasets, and find that these produce higher-quality samples than generators trained against a single discriminator.

1.1 Related Work

Researchers have explored several approaches to improve the stability of GANs for training on higher dimensional images. Instead of optimizing Jensen-Shannon divergence as suggested in the original GAN framework, Energy based GAN [12] and Wasserstein GAN [11] show improvement in the stability by optimizing total variation distance and Earth mover distance respectively, together with regularizing the discriminator to limit the discriminator capacity. [10] further extended GAN training to any choice of f -divergence as objective. [8] proposed several heuristics to improve the stability of training. These include modifying the objective function, virtual batch-normalization, historical averaging of parameters, semi-supervised learning, *etc.*. All of these methods are designed to improve the quality of gradients, and provide additional supervision to the generator. They are therefore complementary to, and can likely be used in combination with, our approach.

Note that prior methods have involved training ensembles of GANs [13], or ensembles of discriminators [14]. However, their goal is different from ours. In our framework, each discriminator is shown only a low-dimensional projection of the data, with the goal of preventing it from being able to perfectly reject generated samples. Crucially, we do not combine the outputs of discriminators directly, but rather compute losses on individual discriminators and average these losses.

Indeed, the idea of combining multiple simple discriminators, *e.g.*, with boosting [15], or mixture-of-experts [16], is a common approach to learning. While these combinations are aimed at building a single strong discriminator, our objective is to maintain a flow of gradients from individual discriminators to the generator. It is also worth noting the work of Bonneel *et al.* [17], who also use low-dimensional projections to deal with high-dimensional probability distributions. However, while they use such projections to efficiently compute Wasserstein distances and optimal transport between two distributions, our goal is to enable stable GAN training in high dimensions.

2 Learning with Multiple Discriminators on Random Projections

GANs [1] traditionally comprise of a generator G that learns to generate samples from a data distribution \mathbb{P}_x , through adversarial training against a single discriminator D as:

$$\min_G \max_D V(D, G) = \mathbb{E}_{x \sim \mathbb{P}_x} [\log D(x)] + \mathbb{E}_{z \sim \mathbb{P}_z} [\log(1 - D(G(z)))], \quad (1)$$

for $x \in \mathbb{R}^d$, $\mathbb{P}_x : \mathbb{R}^d \rightarrow \mathbb{R}_+$, $\int \mathbb{P}_x = 1$, and with \mathbb{P}_z a fixed distribution (typically uniform or Gaussian) for noise vectors $z \in \mathbb{R}^{d'}$, $d' \ll d$. The optimization in (1) is carried out using stochastic gradient descent (SGD), with alternating updates to the generator and the discriminator. While this approach works surprisingly well, instability is common during training, especially when generating high-dimensional data.

As described in [9], this instability is due to the fact that the distributions \mathbb{P}_x corresponding to natural data often have very limited support in the ambient domain of x and $G(z)$. Then, the generator G is unable to learn quickly enough to generate samples from distributions that have significant overlap with this support. This in turn makes it easier for the discriminator D to learn to perfectly separate the generator's samples, at which point the latter is left without useful gradients for further training.

The key idea of our approach is to train a single generator against an array of discriminators. Each discriminator operates on a different low-dimensional linear projection, that is set randomly prior to training. Formally, we train a generator G against multiple discriminators $\{D_k\}_{k=1}^K$ as:

$$\min_G \max_{\{D_k\}} \sum_{i=k}^K V(D_k, G) = \sum_{i=k}^K \mathbb{E}_{x \sim \mathbb{P}_x} [\log D_k(W_k^T x)] + \mathbb{E}_{z \sim \mathbb{P}_z} [\log(1 - D_k(W_k^T G(z)))], \quad (2)$$

where $W_k, k \in \{1, \dots, K\}$ is a random matrix in $\mathbb{R}^{d \times m}$.

As we will show in the following results, the above formulation addresses the issue of instability by ensuring the true marginal distributions of the low-dimensional projections $\{W_k^T x\}$ have comparatively larger support. Consequently, each discriminator D_k is unable to perfectly separate real and generated samples, and continues to provide gradients to the generator. Moreover, we will also show that since the generator must simultaneously match the marginals of \mathbb{P}_x along all projections $\{W_k^T\}$ to minimize the loss in (2), it will learn to generate samples under the true distribution \mathbb{P}_x , given a sufficiently large number of projections K .

2.1 Stability

If the support of the true distribution \mathbb{P}_x occupies a low volume relative to the range of possible values of x , it is hard for the generator to produce samples within that support, which makes it easy for a discriminator to quickly learn to classify all such samples as fake. Here, we argue that this problem is ameliorated by training discriminators on lower-dimensional projections of x and $G(z)$.

For simplicity, we assume that the range of x is the d -dimensional ball B^d of radius 1 centered at 0. We define the support $\text{supp}(\mathbb{P}_x) \subset B^d$ of a distribution \mathbb{P}_x to be the set where the density is greater than some small threshold ϵ . Let $W \in \mathbb{R}^{d \times m}$ be an entry-wise random Gaussian projection matrix. We denote as B_W^d the projection of the range on W , and $\mathbb{P}_{W^T x}$ as the marginal of \mathbb{P}_x along W .

Theorem 2.1. Assume $\mathbb{P}_x = \sum_j \tau_j \mathcal{N}(x|\mu_j, \Sigma_j)$ is a mixture of Gaussians, such that the individual components are sufficiently well separated (in the sense that there is no overlap between their supports or the projections thereof, see [18]). If $\text{supp}(\mathbb{P}_x) \subset B^d$ and $\text{Vol}(\text{supp}(\mathbb{P}_x)) > 0$, then $\text{Vol}(\text{supp}(\mathbb{P}_{W^T x}))/\text{Vol}(B_W^d) > \text{Vol}(\text{supp}(\mathbb{P}_x))/\text{Vol}(B^d)$ with high probability.

The above result, proved in the supplementary, implies that the projection of the support of \mathbb{P}_x occupies a higher fraction of the volume of the projection of the range of x . This aids in stability because a larger fraction of the generator’s samples (which lie within the range of x), after projection, will overlap with the projected support $\text{supp}(\mathbb{P}_x)$, and can not be rejected absolutely by the discriminator.

2.2 Consistency

The following two results, proved in the supplementary, show that with discriminators acting on a sufficiently large number K of random projections, the generator G will learn to produce samples under a distribution that matches the true data distribution \mathbb{P}_x .

Theorem 2.2. Let \mathbb{P}_g denote the distribution of the generator outputs $G(z)$, where $z \sim \mathbb{P}_z$, and let $\mathbb{P}_{W_k^T g}$ be the marginals of \mathbb{P}_g along W_k . For fixed G , the optimal $\{D_k\}$ are given by

$$D_k(y) = \frac{\mathbb{P}_{W_k^T x}(y)}{\mathbb{P}_{W_k^T x}(y) + \mathbb{P}_{W_k^T g}(y)}, \quad (3)$$

for all $k \in \{1, \dots, K\}$. The optimal G that minimizes (2) is achieved iff $\mathbb{P}_{W_k^T x} = \mathbb{P}_{W_k^T g}$, $\forall k$.

The above result implies that the marginals of the distribution of the optimal generator match those of the data distribution along all projections $\{W_k^T\}$. The next theorem states that for any smooth data distribution \mathbb{P}_x , the generator distribution \mathbb{P}_g will be close to \mathbb{P}_x once it matches marginals along a sufficiently large number of projections.

Theorem 2.3. A distribution $\mathbb{P}_x : \mathbb{R}^d \rightarrow \mathbb{R}_+$ is L -Lipschitz, if $\forall x_1, x_2 \in \mathbb{R}^d$, $|\mathbb{P}_x(x_1) - \mathbb{P}_x(x_2)| \leq L \cdot d(x_1, x_2)$. Let \mathbb{P}_x and \mathbb{P}_g be L -Lipschitz and compact distributions with support of radius B , such that $\mathbb{P}_{W_k^T x} = \mathbb{P}_{W_k^T g}$, $\forall k \in \{1, \dots, K\}$. Let $\{W_k\}$ be entrywise random Gaussian matrices in $\mathbb{R}^{d \times m}$. If $K > O((\frac{B \cdot L}{\epsilon})^{d-m})$, then for any $x \in \mathbb{R}^d$, $|\mathbb{P}_x(x) - \mathbb{P}_g(x)| \leq O(\epsilon)$, with high probability.

Note that when the true distribution \mathbb{P}_x is low dimensional, and does not have exponential degrees of freedom as assumed above, a far smaller number of projections K may suffice. As described later in Sec. 3, we find setting K to two to four times d/m to be adequate in our experiments.

2.3 Projections for Generating Image Data

Prior work [6] has shown that using convolutional architectures for both the generator and discriminator networks is key to generating images with GANs. While individual discriminators in our framework see projected inputs that are lower-dimensional than the full image, their dimensionality is still large enough (a very small m would require a large number of discriminators) to make it hard to train discriminators with only fully-connected layers. Therefore, it is desirable to employ convolutional architectures for each discriminator.

To do so, the projection matrices W_k^T must be chosen to produce “image-like” data. Accordingly, we use downsampled convolutions with random filters to embody the projections W_k^T (as illustrated in Fig. 1). The elements of these convolution filters are drawn i.i.d. from a Gaussian distribution, and the filters are then scaled to have unit ℓ_2 norm. Note that this imposes a block-Toeplitz structure on W_k^T , and they are no longer purely random as assumed in above. We partially address this by choosing filter sizes that are larger than the downsampling rate to promote more “mixing” of the input coordinates (e.g., we use 8×8 filters when using a stride of 2). We find that our strategy works well in practice, and that the benefits of using convolutional architectures for each discriminator D_k outweigh the drawbacks of not using projections that are purely random.

3 Experimental Results

In this section, we evaluate our approach with experiments comparing to generators trained against a single discriminator that sees the entire image as input, and demonstrate that it leads to higher stability during training, and ultimately yields generators that produce higher quality samples.

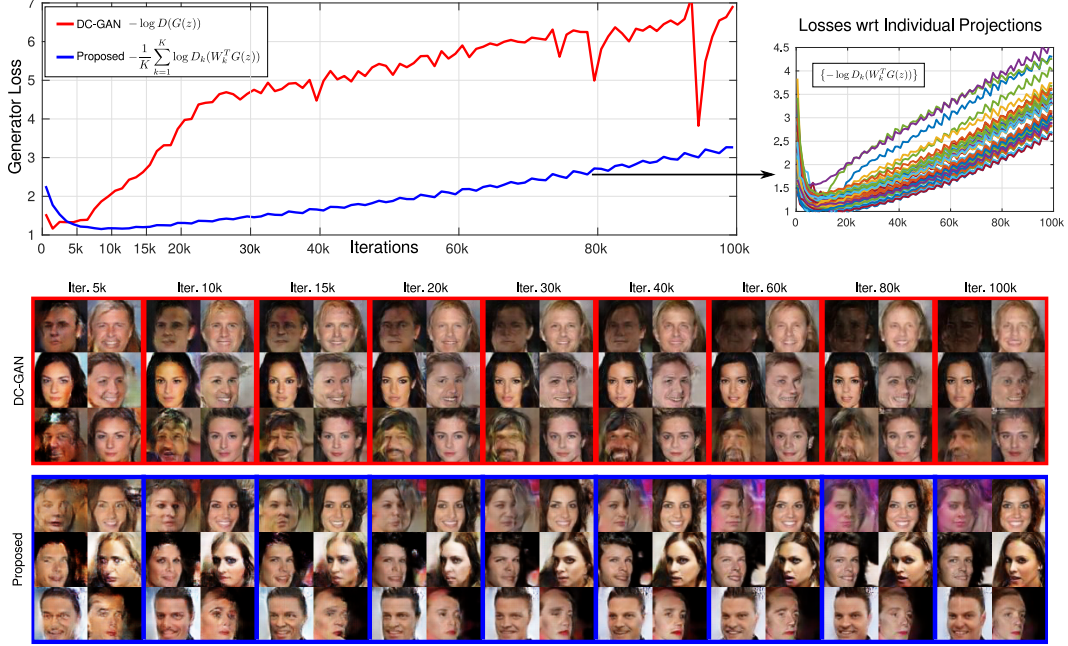


Figure 2: Evolution of generators through training. **(Top)** We plot the losses for generators trained with a single discriminator (DC-GAN), and with multiple discriminators ($K = 48$) in the proposed framework. While the loss increases through training in both cases, our loss—both average and with respect to individual discriminators—remains lower in absolute terms compared to DC-GAN. **(Bottom)** As a consequence, the quality of samples generated from our framework improves continually through training, while samples from traditional DC-GAN begin to deteriorate after a point. At the same time, training against multiple discriminators allows our generator to learn the data distribution quickly, and produce high quality samples even in early iterations.

Dataset and Architectures. For evaluation, we primarily use the dataset of celebrity faces collected by [19]—we use the cropped and aligned 64×64 -size version of the images—and the DC-GAN [6] architectures for the generator and discriminator. We make two minor modifications to the DC-GAN implementation that we find empirically to yield improved results (for both the standard single discriminator setting, as well as our multiple discriminator setting). Firstly, we use different batches of generated images to update the discriminator and generator—this increases the amount of computation required, but yields better quality results and faster training. Secondly, we employ batch normalization in the generator but *not* in the discriminator (the original DC-GAN implementation normalized real and generated batches separately, which we found yielded poorer generators).

For our approach, we train a generator against K discriminators, each operating on a different single-channel 32×32 projected version of the input, *i.e.*, $d/m = 12$. The projected images are generated through convolution with 8×8 filters and a stride of two. The filters are generated randomly and kept constant throughout training. We compare this to the standard DC-GAN setting of a single discriminator that looks at the full-resolution 64×64 color image. We use identical generator architectures in both settings—that map a 100 dimensional uniformly distributed noise vector to a full resolution image. The discriminators also have similar architectures—but each of the discriminator in our setting has one less layer as it operates on a lower resolution input (we map the number of channels in the first layer in our setting to those of the second layer of the full-resolution single-discriminator, thus matching the size of the final feature vector used for classification).

As is standard practice, we compute generator gradients in both settings with respect to minimizing the “incorrect” classification loss of the discriminator—in our setting, this loss is given by $-\frac{1}{K} \sum_k \log D_k(G(z))$. As suggested in [6], we use Adam [20] with learning rate 2×10^{-4} , $\beta_1 = 0.5$, and a batch size of 64.

Stability. We begin by analyzing the evolution of generators in both settings through training. Figure 2 shows the generator training loss for traditional DC-GAN with a single discriminator, and

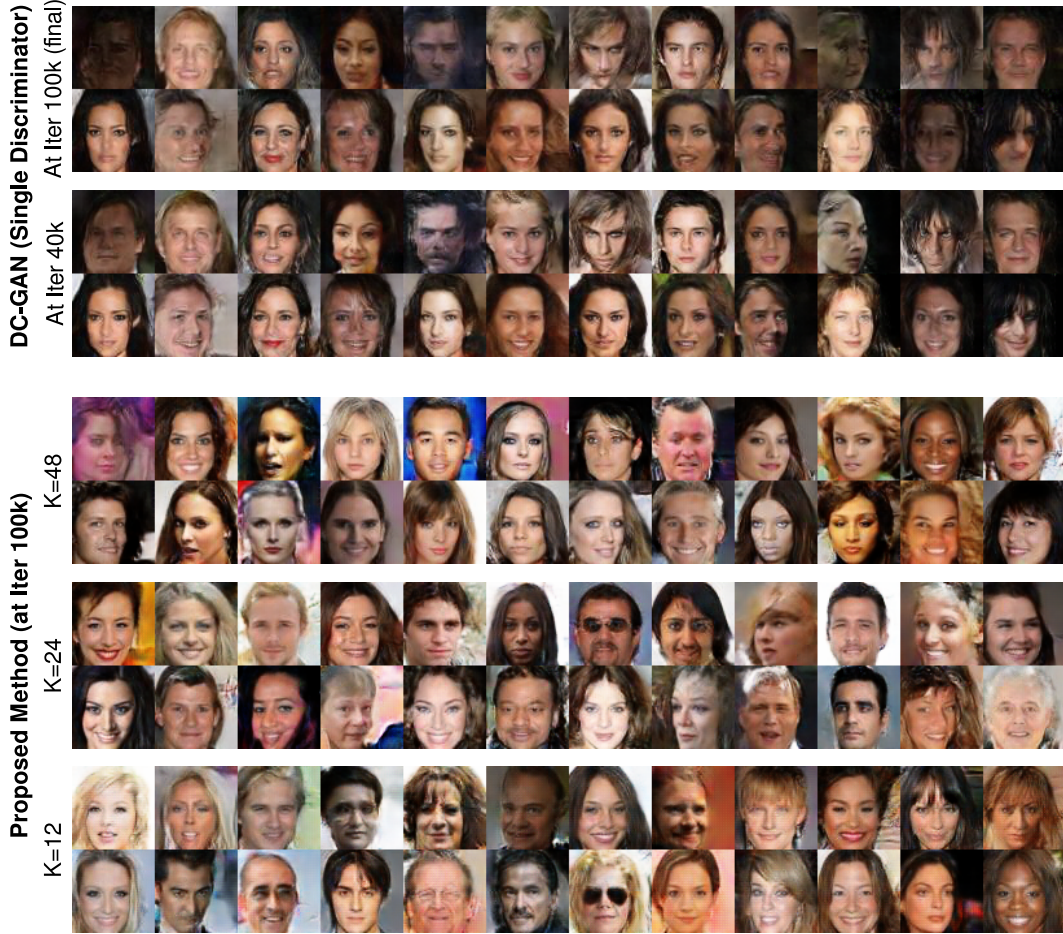


Figure 3: Random sets of generated samples from traditional DC-GAN and the proposed framework. For DC-GAN, we show results from the model both at 40k iterations (when the samples are qualitatively the best) and at the end of training (100k iterations). For our setting, we show samples from the end of training for generator models trained with $K = 12, 24, 48$ projections. We find that our generator learns to produce qualitatively better face images, with finer detail and fewer distortions. We also note that the quality is slightly worse when K only equals the projection ratio $d/m = 12$, with subtle high-frequency noise apparent in the samples. However, these artifacts decrease with increasing K , and setting $K = 24$ and 48 leads to similar, high-quality samples.

compares it the proposed framework with $K = 48$ discriminators—displaying both the average loss, and the loss with respect to individual discriminators. In both settings, the generator losses increase through much of training after decreasing in the initial iterations (*i.e.*, the discriminators eventually “win”). However, DC-GAN’s generator loss remains higher than ours in absolute terms throughout training, and after crossing a certain threshold, begins to exhibit high-magnitude oscillations.

Figure 2 also includes examples of generated samples from both generators across iterations (from the same noise vectors). We observe that DC-GAN’s samples improve mostly in the initial iterations while the training loss is still low, in line with our intuition that generator gradients become less informative as discriminators get stronger. Indeed, we find that as training progresses, the quality of samples from traditional DC-GAN actually begins to decrease after around 40k iterations. In contrast, the generator trained in our framework improves continually throughout training.

Consistency. Beyond stability, Fig. 2 also demonstrates the consistency of our framework. While the average loss in our framework is lower (which could, after all, have been achieved simply with a lower learning rate for the discriminator), we see that this does not impede our generator’s ability to



Figure 4: Interpolating in latent space. For selected pairs of generated faces from our approach (with $K = 48$), we produce a sequence of samples using our model with different convex combinations of their noise vectors. We see that nearly every combination generates a plausible face, and that these smoothly interpolate between various facial attributes—age, gender, race, expression, hair, *etc.* In all cases, the $\alpha = 0.5$ sample clearly corresponds to an individual distinct from the original pair.

learn the data distribution quickly as it collates feedback from multiple discriminators. Indeed, our generator produces higher-quality samples than traditional DC-GAN even in early iterations.

Figure 3 includes a larger number of (random) samples from generators trained with traditional DC-GAN and our setting. For DC-GAN, we include samples from both roughly the end (100k iterations) of training, as well as from roughly the middle (40k iterations) where the sample quality are approximately the best. For our approach, we show results from training with different numbers of discriminators with $K = 12, 24$, and 48 —selecting the generator models from the end of training for all. We see that our generators produce face images with higher-quality detail and far fewer distortions than traditional DC-GAN. We also note the effect of the number of discriminators on sample quality. Specifically, we find that setting K to be equal only to the projection ratio $d/m = 12$ leads to subtle high-frequency noise in the generator samples, suggesting these many projections do not sufficiently constrain the generator to learn the full data distribution. However, increasing K diminishes these artifacts, with both $K = 24$ and $K = 48$ yielding similar, high-quality samples.

Training Time. The improved generator model quality comes at the expense of increased computation during training. While training traditional DC-GAN with a single discriminator takes only 0.6 seconds per iteration (on an NVIDIA Titan X), the iteration time in our framework goes up to 3.2 seconds for $K = 12$, 5.8 seconds for $K = 24$, and 11.2 seconds for $K = 48$. However, since our generator architecture is identical to that in the traditional setting, the time taken to produce samples is the same once training is complete.

Latent Embedding. Next, we explore the quality of the embedding induced by our generator (trained with $K = 48$) in the latent space of noise vectors z . In Fig. 4, we consider selected pairs of randomly generated faces, and generate samples by linear interpolation between their corresponding noise vectors. We find that each of these generated samples is also a plausible face image—this confirms both that our generator is not simply memorizing training samples, and that it is densely packing the latent space with face images. We also find that the generated samples smoothly interpolate between semantically meaningful face attributes—gender, race, age, hair-style, expression, and so on. Note that in all rows, the sample for $\alpha = 0.5$ appears to be a clearly different individual than the ones represented by $\alpha = 0$ and $\alpha = 1$.



Figure 5: Examples from training on canine images from Imagenet. We show manually selected examples of 128×128 images produced by generators trained on a subset of 160k images from classes corresponding to canines. While the images are not globally plausible, we see that the generator learns to reproduce low-level textures, and rough high-level composition.

Results on Imagenet-Canines. Finally, we also use our framework to train a generator on a subset of the Imagenet-1K database [21]. We train on 128×128 image crops (formed by scaling the smaller side to 128, and then taking a random crop along the other dimension), over a subset of Imagenet classes corresponding roughly to canines—from classes 152 (*chihuahua*) to 281 (grey fox), with 160k images. We largely use the same settings as for faces. However, we feed a higher 200-dimensional noise vector to the generator, which also begins by mapping this to a feature vector that is twice as large (2048), and which has an extra transpose-convolution layer to go upto the 128×128 resolution. We again use convolutional 8×8 filters with stride two to form our projection matrices $\{W_k^T\}$, but in this case, these projections map to 64×64 single channel images. Due to time constraints, we use only $K = 12$ discriminators. Each discriminator also has an additional layer because of the higher-resolution, but we reduce the number of channels in the first layer such that the feature vector used for classification is the same dimensionality as that in our face experiments.

Figure 5 shows selected samples after 100k iterations of training (note that these are manually selected samples, please see the supplementary material for a larger random set). We see that since it is trained on a more diverse and unaligned image content, the generated images are not globally plausible photographs. Nevertheless, we find that the produced images are sharp, and that generator learns to reproduce realistic low-level textures as well as some high-level composition.

4 Conclusion

In this paper, we proposed a new framework for training GANs with high-dimensional outputs. Our approach employs multiple discriminators on random projections of the data to stabilize training, with enough projections to ensure that the generator learn the true data distribution. Experimental results demonstrate that generators trained using our method are in fact more stable—they continue to learn throughout training while those trained against a single discriminator often diverge, and produce higher-quality samples that match the true data distribution. Source code and trained models for our implementation is available at the project page <http://www.ttic.edu/chakrabarti/rpgan/>.

In our current framework, the number of discriminators is limited by computational cost. In future work, we plan to investigate training with a much larger set of discriminators, employing only a small subset of them at each iteration, or every set of iterations. We are also interested in using multiple discriminators with modified and regularized objectives (e.g., [10–12]). Such modifications are complementary to our approach, and deploying them together will likely be beneficial.

Acknowledgments: AC was supported by the National Science Foundation under award no. IIS:1618021, and also thanks NVIDIA corporation for the donation of a Titan X GPU that was used in this research.

References

- [1] Ian Goodfellow, Jean Pouget-Abadie, Mehdi Mirza, Bing Xu, David Warde-Farley, Sherjil Ozair, Aaron Courville, and Yoshua Bengio. Generative adversarial nets. In *NIPS*, 2014.

- [2] Emily Denton, Sam Gross, and Rob Fergus. Semi-supervised learning with context-conditional generative adversarial networks. *arXiv:1611.06430 [cs.CV]*, 2016.
- [3] Christian Ledig, Lucas Theis, Ferenc Huszár, Jose Caballero, Andrew Cunningham, Alejandro Acosta, Andrew Aitken, Alykhan Tejani, Johannes Totz, Zehan Wang, and Wenzhe Shi. Photo-realistic single image super-resolution using a generative adversarial network. *arXiv:1609.04802 [cs.CV]*, 2016.
- [4] Phillip Isola, Jun-Yan Zhu, Tinghui Zhou, and Alexei A Efros. Image-to-image translation with conditional adversarial networks. *arXiv:1611.07004 [cs.CV]*, 2016.
- [5] Xi Chen, Yan Duan, Rein Houthoofd, John Schulman, Ilya Sutskever, and Pieter Abbeel. Infogan: Interpretable representation learning by information maximizing generative adversarial nets. In *NIPS*, 2016.
- [6] Alec Radford, Luke Metz, and Soumit Chintala. Unsupervised representation learning with deep convolutional generative adversarial networks. In *ICLR*, 2016.
- [7] Emily L Denton, Soumith Chintala, Rob Fergus, et al. Deep generative image models using a laplacian pyramid of adversarial networks. In *NIPS*, 2015.
- [8] Tim Salimans, Ian Goodfellow, Wojciech Zaremba, Vicki Cheung, Alec Radford, and Xi Chen. Improved techniques for training gans. In *NIPS*, 2016.
- [9] Martin Arjovsky and Léon Bottou. Towards principled methods for training generative adversarial networks. In *NIPS Workshop on Adversarial Training*, 2016.
- [10] Sebastian Nowozin, Botond Cseke, and Ryota Tomioka. f-gan: Training generative neural samplers using variational divergence minimization. In *NIPS*, 2016.
- [11] Martin Arjovsky, Soumith Chintala, and Léon Bottou. Wasserstein gan. *arXiv:1701.07875 [stat.ML]*, 2017.
- [12] Junbo Zhao, Michael Mathieu, and Yann LeCun. Energy-based generative adversarial network. *arXiv:1609.03126 [cs.LG]*, 2016.
- [13] Yaxing Wang, Lichao Zhang, and Joost van de Weijer. Ensembles of generative adversarial networks. *arXiv:1612.00991 [cs.CV]*, 2016.
- [14] Ishan Durugkar, Ian Gemp, and Sridhar Mahadevan. Generative multi-adversarial networks. *arXiv:1611.01673 [cs.LG]*, 2016.
- [15] Yoav Freund, Robert E Schapire, et al. Experiments with a new boosting algorithm. In *ICML*, 1996.
- [16] Robert A Jacobs. Methods for combining experts’ probability assessments. *Neural computation*, 1995.
- [17] Nicolas Bonneel, Julien Rabin, Gabriel Peyré, and Hanspeter Pfister. Sliced and radon wasserstein barycenters of measures. *Journal of Mathematical Imaging and Vision*, 2015.
- [18] Sanjoy Dasgupta. Learning mixtures of gaussians. In *Foundations of Computer Science*. IEEE, 1999.
- [19] Ziwei Liu, Ping Luo, Xiaogang Wang, and Xiaoou Tang. Deep learning face attributes in the wild. In *ICCV*, 2015.
- [20] Diederik Kingma and Jimmy Ba. Adam: A method for stochastic optimization. *arXiv preprint arXiv:1412.6980*, 2014.
- [21] Jia Deng, Wei Dong, Richard Socher, Li-Jia Li, Kai Li, and Li Fei-Fei. Imagenet: A large-scale hierarchical image database. In *CVPR*, 2009.
- [22] Roman Vershynin. Introduction to the non-asymptotic analysis of random matrices. *arXiv:1011.3027 [math.PR]*, 2010.

Supplementary Material

A Proofs

Proof of Theorem 2.1. We first show that we can assume that the columns of the projection W are orthonormal. Since $W \in \mathbb{R}^{d \times m}$ is entry-wise Gaussian distributed, it has rank m with high probability. Then, there exists a square invertible matrix A such that $W' = AW$ where W' is orthonormal. In that case, $\text{Vol}(\text{supp}(\mathbb{P}_{W^T x})) / \text{Vol}(B_W^d) = \text{Vol}(\text{supp}(\mathbb{P}_{W'^T x})) / \text{Vol}(B_{W'}^d)$ because the numerator and denominator terms for both can be related by $\det(A)$ for the change of variables, which cancels out. Note that under this orthonormal assumption, $B_W^d = B^m$.

Next, we consider the case of an individual Gaussian distribution $\mathbb{P}_x = \mathcal{N}(x|\mu, \Sigma)$, and prove that the ratio of supports (defined with respect to a threshold ϵ) does not decrease with the projection. The expression for these ratios is given by:

$$\begin{aligned} \text{Vol}(\text{supp}(\mathbb{P}_x)) &= \text{Vol}(B^d) \times \det(\Sigma) \times \left[\log \frac{1}{\epsilon^2} - d \log 2\pi - \log \det(\Sigma) \right] \\ \Rightarrow \frac{\text{Vol}(\text{supp}(\mathbb{P}_x))}{\text{Vol}(B^d)} &= \det(\Sigma) \times \left[\log \frac{1}{\epsilon^2} - d \log 2\pi - \log \det(\Sigma) \right]. \end{aligned} \quad (4)$$

$$\frac{\text{Vol}(\text{supp}(\mathbb{P}_{W^T x}))}{\text{Vol}(B_W^d)} = \det(W^T \Sigma W) \times \left[\log \frac{1}{\epsilon^2} - m \log 2\pi - \log \det(W^T \Sigma W) \right]. \quad (5)$$

For sufficiently small ϵ , the volume ratio of a single Gaussian will increase with projection if $\det(W^T \Sigma W) > \det(\Sigma)$. Note that all eigenvalues of $\Sigma \leq 1$, with at-least one eigenvalue strictly < 1 (since $\text{supp}(\mathbb{P}_x) \subset B^d$). First, we consider the case when Σ is not strictly positive definite and one of the eigenvalues is 0. Then, $\text{Vol}(\text{supp}(\mathbb{P}_x)) = 0$ and $\text{Vol}(\text{supp}(\mathbb{P}_{W^T x})) \geq 0$, i.e., the volume ratio either stays the same or increases.

For the case when all eigenvalues are strictly positive, consider a co-ordinate transform where the first m co-ordinates of x correspond to the column vectors of W , such that

$$\Sigma = \begin{bmatrix} \Sigma_W & \Sigma_{WW'} \\ \Sigma_{WW'}^T & \Sigma_{W'} \end{bmatrix}, \quad (6)$$

where $\Sigma_W = W^T \Sigma W$. Then,

$$\begin{aligned} \det(\Sigma) &= \det(\Sigma_W) \det(\Sigma_{W'} - \Sigma_{WW'}^T \Sigma_W^{-1} \Sigma_{WW'}) \\ &\leq \det(\Sigma_W) \det(\Sigma_{W'}), \\ \Rightarrow \det(\Sigma_W) &\geq \det(\Sigma) / \det(\Sigma_{W'}). \end{aligned} \quad (7)$$

Note that $\det(\Sigma_{W'}) \leq 1$, since all eigenvalues of Σ are ≤ 1 , with equality only when W is completely orthogonal to the single eigenvector whose eigenvalue is strictly < 1 , which has probability zero under the distribution for W . Therefore, we have that $\det(\Sigma_{W'}) < 1$, and

$$\det(W^T \Sigma W) = \det(\Sigma_W) > \det(\Sigma). \quad (8)$$

The above result shows that the volume ratio of individual components never decrease, and *always* increase when their co-variance matrices are full rank (no zero eigenvalue). Now, we consider the case of the Gaussian mixture. Note that the volume ratio of the mixture equals the sum of the ratios of individual components, since the denominator $\text{Vol}(B^m)$ is the same, where the support volume in these ratios for component j is defined with respect to a threshold ϵ/τ_j . Also, note that since mixture distribution has non-zero volume, at least one of the Gaussian components must have all non-zero eigenvalues. Therefore, the volume ratios of \mathbb{P}_x and $\mathbb{P}_{W^T x}$ are both sums of individual Gaussian component terms, and each term for $\mathbb{P}_{W^T x}$ is greater than or equal to the corresponding term for \mathbb{P}_x , and at least one term is strictly greater. Therefore, the support volume ratio of $\mathbb{P}_{W^T x}$ is strictly greater than that of \mathbb{P}_x .

Proof of Theorem 2.2. The proof of follows along the same steps as that of Theorem 1 in [1].

$$\begin{aligned}
V(D_k, G) &= \mathbb{E}_{x \sim \mathbb{P}_x} [\log D_k(W_k^T x)] + \mathbb{E}_{x \sim \mathbb{P}_g} [\log(1 - D_k(W_k^T x))] \\
&= \mathbb{E}_{Y \sim \mathbb{P}_{W_k^T x}} [\log D_k(y)] + \mathbb{E}_{y \sim \mathbb{P}_{W_k^T g}} [\log(1 - D_k(y))]. \tag{9}
\end{aligned}$$

For any point $y \in \text{supp}(\mathbb{P}_{W_k^T x}) \cup \text{supp}(\mathbb{P}_{W_k^T g})$, differentiating $V(D_k, G)$ w.r.t. D_k and setting to 0 gives us:

$$D_k(y) = \frac{\mathbb{P}_{W_k^T x}(y)}{\mathbb{P}_{W_k^T x}(y) + \mathbb{P}_{W_k^T g}(y)}. \tag{10}$$

Notice we can rewrite $V(D_k, G)$ as

$$\begin{aligned}
V(D_k, G) &= -2 \log(2) + KL \left(\mathbb{P}_{W_k^T x} \parallel \frac{\mathbb{P}_{W_k^T x} + \mathbb{P}_{W_k^T g}}{2} \right) \\
&\quad + KL \left(\mathbb{P}_{W_k^T g} \parallel \frac{\mathbb{P}_{W_k^T x} + \mathbb{P}_{W_k^T g}}{2} \right). \tag{11}
\end{aligned}$$

Here KL is the Kullback Leibler divergence, and it is easy to see that the above expression achieves the minimum value when $\mathbb{P}_{W_k^T x} = \mathbb{P}_{W_k^T g}$.

Proof of Theorem 2.3. We first prove this result for discrete distributions supported on a compact set \mathcal{S} with γ points along each dimension. Let $\tilde{\mathbb{P}}$ denote such a discretization of a distribution \mathbb{P} .

Each of the marginal equation $\tilde{\mathbb{P}}_{W_k^T x} = \tilde{\mathbb{P}}_{W_k^T g}$ is equivalent to γ^m linear equations of the distribution $\tilde{\mathbb{P}}_x$ of the form, $\sum_{x: W_k^T x = y} \tilde{\mathbb{P}}_x(x) = \tilde{\mathbb{P}}_{W_k^T g}(y)$. Note that we have γ^d choices for x and γ^m choices for y . Let $A_k \in \mathbb{R}^{\gamma^m \times \gamma^d}$ denote the coefficient matrix $A_k \tilde{\mathbb{P}}_x = \tilde{\mathbb{P}}_{W_k^T g}$, such that $A_k(i, j) = 1$ if $W_k^T x_i = y_j$, and 0 otherwise.

The rows of A_k for different values of y_j are clearly orthogonal. Further, since different W_k are independent Gaussian matrices, rows of A_k corresponding to different W_k are linearly independent. In particular let $A \in \mathbb{R}^{\gamma^m K \times \gamma^d}$ denote the vertical concatenation of A_k . Then, A has full row rank of $\gamma^m \cdot K$ with probability $\geq 1 - c \cdot m \cdot e^{-d}$ [22]. Here c is some arbitrary positive constant.

Since $\tilde{\mathbb{P}}_x$ is a vector of dimension γ^d , that many linearly independent equations, uniquely determine it. Hence $\gamma^m \cdot K \geq \gamma^d$, guarantees that $\tilde{\mathbb{P}}_x = \tilde{\mathbb{P}}_g$.

Now we extend the results to the continuous setting. Without loss of generality, let the compact support \mathcal{S} of the distributions be contained in a sphere of radius B . Let $\mathcal{N}_{\frac{\epsilon}{L}}$ be an $\frac{\epsilon}{L}$ net of \mathcal{S} , with γ^d points (see Lemma 5.2 in [22]), where $\gamma = 2B \cdot L/\epsilon$. Then for every point $x_1 \in \mathcal{S}$, there exists a $x_2 \in \mathcal{N}_{\frac{\epsilon}{L}}$ such that, $d(x_1, x_2) \leq \frac{\epsilon}{L}$.

Further for any x_1, x_2 with $d(x_1, x_2) \leq \frac{\epsilon}{L}$, from the Lipschitz assumption of the distributions we know that,

$$|\mathbb{P}_x(x_1) - \mathbb{P}_x(x_2)| \leq L \cdot \frac{\epsilon}{L} = \epsilon. \tag{12}$$

Finally, notice that the marginal constraints do not guarantee that the distributions $\tilde{\mathbb{P}}_{W_k^T x}$ and $\tilde{\mathbb{P}}_{W_k^T g}$ match exactly on the ϵ -net, but only that they are equal upto an additive factor of ϵ . Hence, combining this with equation 12 we get,

$$|\mathbb{P}_x(x) - \mathbb{P}_g(x)| \leq O(\epsilon),$$

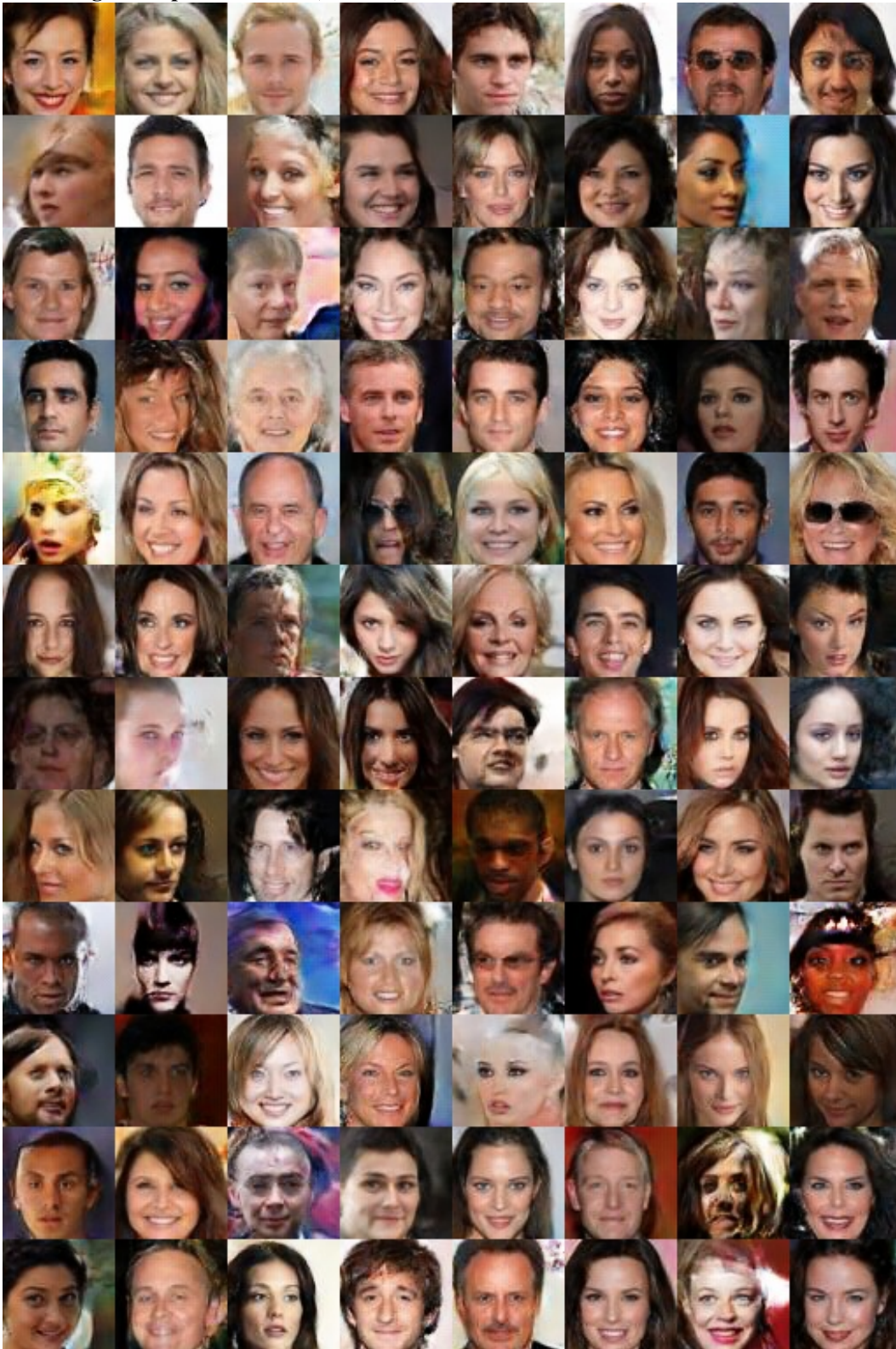
for any x with probability $\geq 1 - c \cdot m \cdot K \cdot e^{-d}$.

B Additional Experimental Results

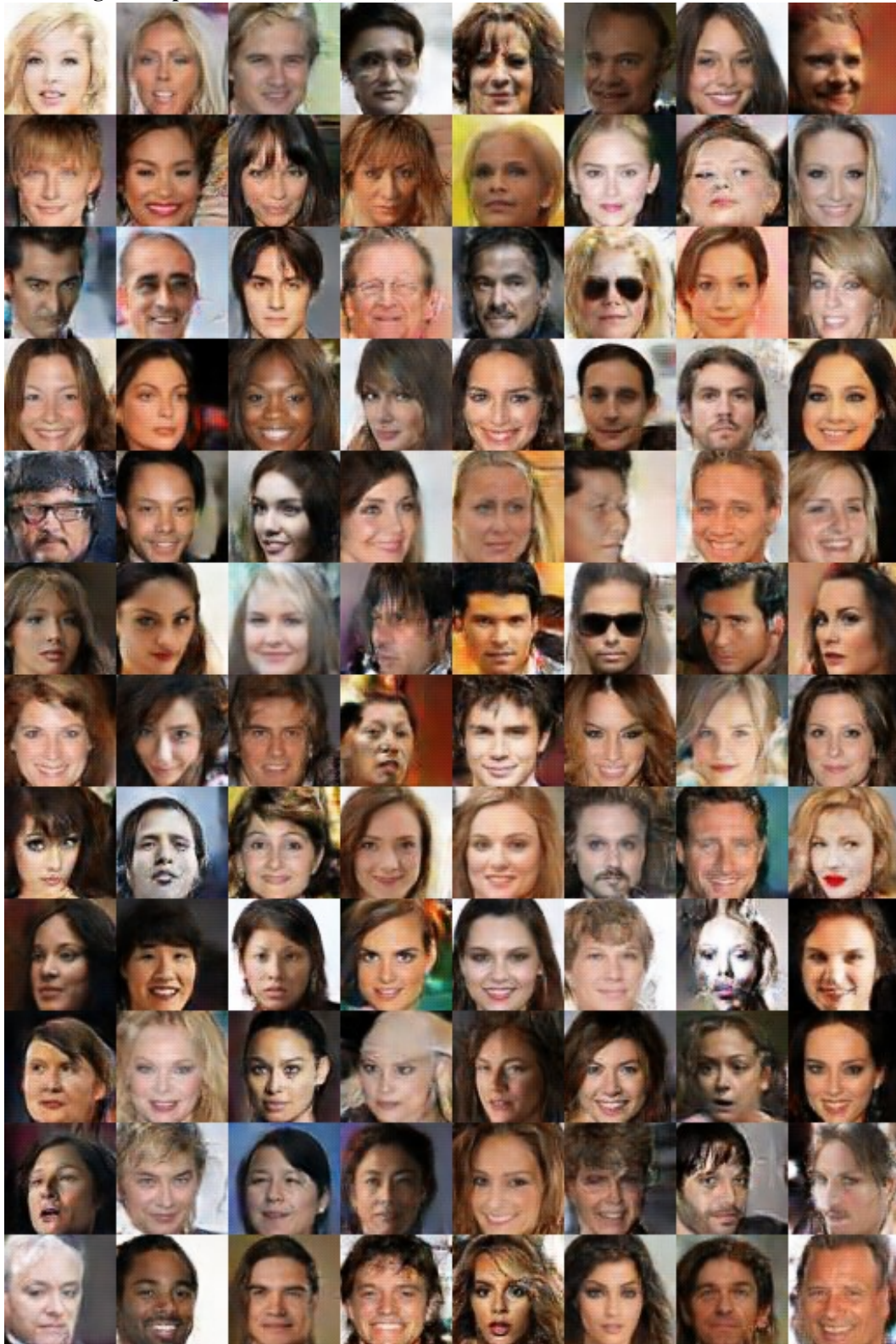
Face Images: Proposed Method ($K = 48$)



Face Images: Proposed Method ($K = 24$)



Face Images: Proposed Method ($K = 12$)



Face Images: Traditional DC-GAN (Iter. 40k)



Face Images: Traditional DC-GAN (Iter. 100k)



Random Imagenet-Canine Images: Proposed Method

